Dalton Transactions

PAPER

View Article Online
View Journal | View Issue

Cite this: *Dalton Trans.*, 2014, **43**, 3372

Binding multidentate ligands to Ni^{2+}: kinetic identification of preferential binding sites†

Dilek Nartop,*[a] William Clegg,[b] Ross W. Harrington,[b] Richard A. Henderson*[b] and Corinne Y. Wills[b]

Received 28th November 2013,
Accepted 17th December 2013

DOI: 10.1039/c3dt53359j

www.rsc.org/dalton

The kinetics of the reactions between $[Ni(MeOH)_6]^{2+}$ (hereafter Ni^{2+}) and a variety of neutral Schiff base multidentate ligands have been measured in methanol at 25.0 °C using stopped-flow spectrophotometry. The ligands contain a variety of different potential donor sites (phenolic OH, imine N, pyridyl N and NH groups), different structural components and substituents. The kinetic studies explore how systematic changes to the composition of the ligands affect the rates of binding. The results are consistent with the Eigen–Wilkins mechanism in which the ligand initially forms an outer-sphere association with Ni^{2+} prior to dissociation of a coordinated solvent molecule and binding to the metal ion. The general features that emerge from these studies are as follows. (i) For ligands with the same donor set, the rates of binding are all similar irrespective of changes to the ligand framework (bridge and substituents). (ii) Comparison of structurally analogous ligands shows that the presence of pyridyl or NH groups in the multidentate results in significantly faster reactions. (iii) With ligands containing multiple NH groups, the rate of ligand binding increases as the number of NH groups increases. The extent to which these kinetic features can be attributed to preferential binding of particular donor groups is discussed.

Introduction

The kinetics of the reactions of multidentate ligands binding to metal ions can obviously be more complicated than the reactions of unidentate ligands because of the multi-stage time courses associated with coordination of the large number of sites.[1,2] An intriguing aspect of the reaction mechanisms with multidentate ligands containing a variety of different types of donor groups is whether the metal discriminates between the various donors and preferentially binds to one type of site. Recent studies have explored the binding of Cu^{2+} to the polytopic ligands shown in Fig. 1 and observed different types of reactivity.[3,4] For the phenanthroline-based ligand (^{phen}L), Cu^{2+} initially binds to the phenanthroline residue and subsequently moves into a macrocyclic cavity. In contrast, for the analogous pyridyl-based ligand, ^{py}L, the pyridyl-residue appears to be just a spectator, with the Cu^{2+} going directly to the macrocyclic cavity. Similar behaviour, in which a metal ion initially binds at one site before moving to its final residence, has been observed with other polytopic ligands.[5,6]

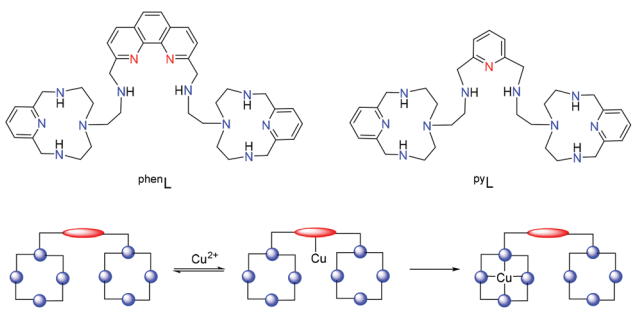

Fig. 1 Structures of polytopic ligands ^{phen}L and ^{py}L and representation of the pathway for incorporation of Cu^{2+} into the macrocyclic cavity for ^{phen}L.

Important questions which need to be addressed are whether binding of metal ions to multidentate ligands (containing various types of donors) involves preferential binding at a specific site, and whether this can be detected using kinetics. In this paper we report kinetic studies on the reactions of $[Ni(MeOH)_6]^{2+}$ (hereafter written as Ni^{2+}) with a variety of neutral multidentate Schiff base ligands (Fig. 2) and investigate if the differences in rates can be attributed to preferential binding of different donors to Ni^{2+}.

[a]*Nevşehir University, Nevşehir, Turkey. E-mail: dileknartop@nevsehir.edu.tr; Fax: +90 384 215 39 48; Tel: +90 384 215 39 00*
[b]*Newcastle University, Newcastle upon Tyne, United Kingdom. E-mail: richard.henderson@ncl.ac.uk; Fax: +44 (0)191 222 6929; Tel: +44 (0)191 222 6636*

†Electronic supplementary information (ESI) available: Tables of spectroscopic and kinetic data; full crystallographic details in CIF format. CCDC 959697–959699. For ESI and crystallographic data in CIF or other electronic format see DOI: 10.1039/c3dt53359j

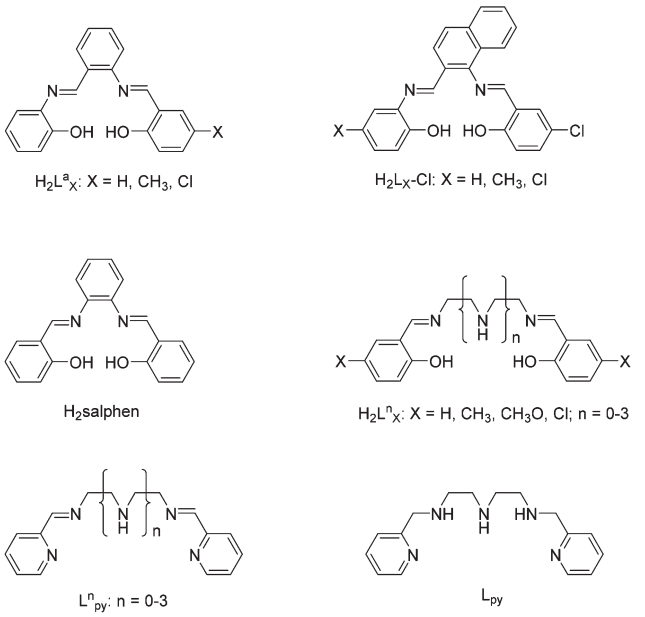

Fig. 2 Structures of the ligands used in this study and the abbreviations used.

Schiff bases and their metal complexes have been studied widely due to their important chemical and biological applications.[7–11] Recently, unsymmetrical Schiff base ligands ($H_2L^a_X$) were reported, and herein the similar ligands H_2L_X–Cl are reported.[12,13]

$H_2L^a_X$, H_2L_X–Cl, $H_2L^n_X$ and L^n_{py} have structures in which there are different types of binding sites: imine nitrogen, terminal phenolic, terminal pyridyl and NH groups. In this paper we present kinetic studies which indicate that the quadridentate ligands $H_2L^a_X$, H_2L_X–Cl, H_2salphen and $H_2L^0_X$ all have very similar reactivities with only minor modulation of the reactivity which is attributable to subtle changes in the outer-sphere association of the ligand with Ni^{2+}, prior to binding. However, for L^n_{py} (where a pyridyl formally replaces a phenol group of $H_2L^n_H$) binding is about 10^3 times faster. Furthermore, introduction of NH groups into either the pyridyl- or salicaldimine-based ligands results in an increase in the rate. The origin of these labilising effect has been explored.

Experimental

All chemicals were purchased from Aldrich or Merck and used without further purification. Elemental analyses were determined using a Leco CHNS-932 analyzer. IR spectra were recorded using a Mattson-5000 FT-IR instrument with KBr pellets. UV-visible absorption spectra were recorded on a Perkin Elmer spectrophotometer. ^{1}H-NMR spectra were carried out on a Bruker Avance 500 MHz or a Bruker Avance 300 MHz instrument. MS analysis was performed using an Agilent Technologies 6410 Triple Quad instrument.

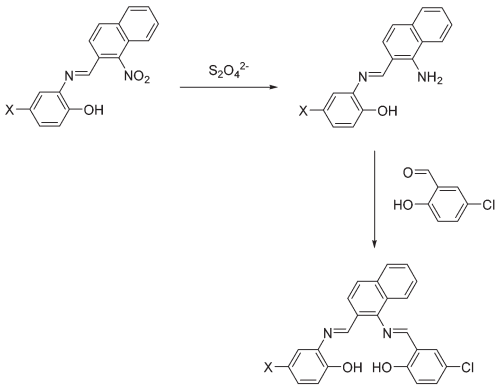

Fig. 3 Synthesis of unsymmetric diimines (H_2L_H–Cl, H_2L_{Me}–Cl, H_2L_{Cl}–Cl).

Synthesis of unsymmetrical Schiff bases H_2L_X–Cl (X = H, Me or Cl): general procedure

The Schiff bases HL_H (or HL_{Me} or HL_{Cl}) were synthesized by adding 50 mmol of 2-aminophenol (or 2-amino-4-methylphenol or 2-amino-4-chlorophenol) to a stirred solution of 1-nitro-2-naphthaldehyde (50 mmol) in ethanol (100 mL) and heating for 1 hour at 60 °C (Fig. 3). The unsymmetrical Schiff bases (H_2L_H–Cl, H_2L_{Me}–Cl, H_2L_{Cl}–Cl) were prepared by using a two-stage method, as shown in Fig. 3. In the first stage, 2 mmol of the Schiff base HL_H (or HL_{Me} or HL_{Cl}) was dissolved in 100 mL ethanol–water solution (1 : 1) at 70 °C. The nitro group of these Schiff bases was reduced to an amino group with solid sodium dithionite as reducing agent. In this reduction process, 5 mmol of solid sodium dithionite was slowly added to the solution in small portions over the course of 1 hour, then the solution was stirred for a further 1 hour at 45–50 °C. In this way the amino derivative of the Schiff bases (A) was obtained in solution. In the second stage, 2 mmol of 2-hydroxy-5-chlorobenzaldehyde in 25 mL ethanol was added to the solution of the amino derivative and was heated to reflux for 2 hours. The mixture was evaporated at room temperature in about 1 day. The orange product was treated with warm water and filtered. The crude product was recrystallized from ethanol. The elemental analyses and mass spectral data for H_2L_X–Cl are presented in Table 1 and the ^{1}H NMR and IR spectra of the compounds are presented in Table 2.[14]

Synthesis of unsymmetrical Schiff bases $H_2L^a_X$ (X = H, Me or Cl): general procedure

One of us recently reported the synthesis and characterization of the unsymmetrical Schiff bases, $H_2L^a_X$, together with some of their metal complexes.[11] The unsymmetrical Schiff bases were prepared by the method described in the literature and shown in Fig. 4. Initially, 2-hydroxy-*N*-(2-nitrobenzylidene)-aniline was obtained by reacting 2-hydroxyaniline (50 mmol) with 2-nitro-benzaldehyde (50 mmol) in ethanol (100 mL) as described previously.[15,16] Subsequently, the nitro group of (B) was reduced to an amino group using sodium dithionite (5 mmol) as reducing agent, in solution. Finally, 1 mmol of

Table 1 Elemental analyses and mass spectral data for H_2L_X–Cl

Compound[a]	Formula	Elemental analysis (calc.) %			Mass spectrum		
		C	N	H	*m/z*	%	Peak
H_2L_H–Cl	$C_{24}H_{17}N_2O_2Cl$	70.05 (71.91)	4.22 (4.24)	6.37 (6.99)	399.2	7.9	$[M]^+$
H_2L_{Me}–Cl	$C_{25}H_{19}N_2O_2Cl$	70.24 (72.38)	4.07 (4.58)	6.39 (6.76)	413.2	22.1	$[M - H]^+$
H_2L_{Cl}–Cl	$C_{24}H_{16}N_2O_2Cl_2$	65.13 (66.21)	4.39 (3.68)	6.85 (6.44)	433.0	18.4	$[M - 2H]^+$

[a] All compounds are orange.

Table 2 The IR vibration frequencies (cm^{-1}) and ^{1}H-NMR chemical shift (ppm) of the unsymmetrical diimines H_2L_X–Cl[a]

Compound	IR					^{1}H-NMR		
	ν(OH)	$\nu(CH)_{arom.}$	ν(C=N)	$\nu(C{=}C)_{ring}$	OH	CH=N	Arom.-H	CH_3
H_2L_H–Cl	3411	3066	1624, 1611	1589–1454	13.81 (d) 1H 10.23 (s) 1H	9.85 (d) 1H 8.96 (d) 1H	6.96–8.41 (m)	—
H_2L_{Me}–Cl	3406	3044	1611, n.o.	1546–1462	13.87 (s) 1H 9.90 (s) 1H	9.57 (s) 1H 8.31 (s) 1H	6.98–8.41 (m)	2.50 (s)
H_2L_{Cl}–Cl	3367	3056	1608, 1589	1547–1461	13.39 (s) 1H 10.07 (s) 1H	9.85 (s) 1H 8.97 (s) 1H	6.57–8.45 (m)	—

[a] s = singlet, d = doublet, m = multiplet, n.o. = not observed.

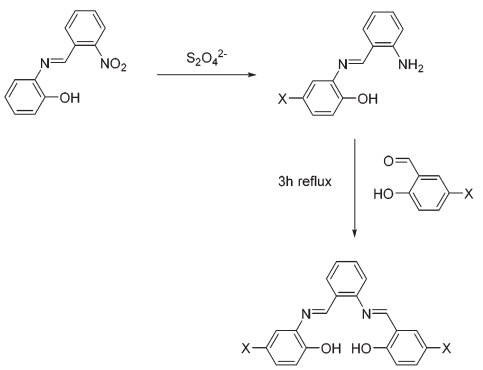

Fig. 4 Synthesis of unsymmetrical diimines ($H_2L^a_H$, $H_2L^a_{Me}$, $H_2L^a_{Cl}$).

2-hydroxybenzaldehyde (or 2-hydroxy-5-methylbenzaldehyde or 2-hydroxy-5-chlorobenzaldehyde) in ethanol (25 mL) was added to the solution to obtain the unsymmetrical diimines, $H_2L^a_H$, $H_2L^a_{Me}$ or $H_2L^a_{Cl}$. Spectroscopic data for all $H_2L^a_X$ have already been reported.[11]

Synthesis of symmetrical Schiff bases $H_2L^n_H$ (n = 0–3): general procedure

All $H_2L^n_H$ were prepared by the same general procedure. A solution of salicaldehyde (4.25 mL; 40 mmol) in ethanol (50 mL) was heated to boiling. The polyamine (20 mmol) was added dropwise to the boiling, stirred solution. The solution turned bright yellow and was stirred for a further 5 minutes then left to cool. Upon cooling yellow crystals of the product formed. The crystals were removed by filtration, washed with diethyl ether and dried in air. Yields of the compounds were all in the range 83–92%. The spectroscopic characterization of these ligands is presented in the ESI.†

Synthesis of Ni^{II} complexes with unsymmetrical diimines $H_2L^a_X$ and symmetrical diimines $H_2L^n_H$: general procedure

All the complexes were prepared by the same general procedure. A solution of the Schiff base ligand (5.0 mmol) in methanol (30 mL) was prepared in a round-bottom flask. A solution of $NiCl_2{\cdot}6H_2O$ (5 mmol) in methanol (30 mL) was then added to the ligand solution. The mixture immediately became a brown/orange colour. The mixture was stirred and heated for about 1 hour, maintaining the temperature at less than 75 °C. The solution was then allowed to cool. Volatiles were removed *in vacuo* until incipient crystallization. The solid was removed by filtration, washed with diethyl ether and dried in air. The solid was recrystallized by dissolving in the minimum volume of methanol, then layering diethyl ether (about 4–5 times the volume of methanol) on top. The purified products were all dark orange/brown complexes. The spectroscopic characterization of these complexes is presented in the ESI.†

X-Ray crystallography

Data for $[NiCl(L_{py})]Cl$ were collected on a Bruker SMART 1 K diffractometer, those for $[Ni(HL^1_H)]Cl{\cdot}CH_3OH$ and $[\{NiCl(L^1_{py})\}_2]Cl_2{\cdot}2CH_3OH{\cdot}2H_2O$ on an Oxford Diffraction (now Agilent Technologies) Gemini A Ultra diffractometer. All measurements were made at 150 K with Mo Kα radiation (λ = 0.71073 Å). Semi-empirical absorption corrections were applied, based on repeated and symmetry-equivalent reflections. The structures were solved by direct methods, and refined on all F^2 values. H atoms bonded to ordered heteroatoms were refined freely; a riding model was used for other H atoms. Crystal and refinement data are presented in Table 3. Disorder was resolved for the unique methanol solvent molecule in $[\{NiCl(L^1_{py})\}_2]Cl_2{\cdot}2CH_3OH{\cdot}2H_2O$. Diffraction for the

Table 3 X-ray crystallographic data

Compound	$[Ni(HL^1_H)]Cl$	$[NiCl(L_{py})]Cl{\cdot}CH_3OH$	$[\{NiCl(L^1_{py})\}_2]Cl_2{\cdot}2CH_3OH{\cdot}2H_2O$
Formula	$C_{18}H_{19}ClN_3NiO_2$	$C_{17}H_{27}Cl_2N_5NiO$	$C_{34}H_{50}Cl_4N_{10}Ni_2O_4$
M_r/g mol^{-1}	403.5	447.0	922.1
Crystal system	Monoclinic	Monoclinic	Triclinic
Space group	$P2_1/c$	$P2_1/c$	$P\bar{1}$
a/Å	10.8103(12)	13.9076(7)	9.2913(5)
b/Å	14.5972(12)	11.3295(5)	10.2003(5)
c/Å	12.1913(14)	14.1620(7)	12.0495(7)
α/°	90	90	83.850(4)
β/°	114.061(13)	117.8704(8)	67.556(5)
γ/°	90	90	82.657(4)
V/Å^3	1756.6(4)	1972.62(16)	1044.70(10)
Z	4	4	1
D_{calc}/g cm^{-3}	1.530	1.505	1.466
μ/mm^{-1}	1.27	1.27	1.21
Min., max. transmission	0.890, 0.950	0.700, 0.800	0.804, 0.890
Reflections measured	5795	11 514	10 097
Unique reflections, R_{int}	3100, 0.0613	4799, 0.0335	4900, 0.0221
Refined parameters	234	252	266
R (F, $F^2 > 2\sigma$)	0.0856	0.0348	0.0236
R_w (F^2, all data)	0.2425	0.0776	0.0609
Goodness of fit on F^2	1.022	1.063	1.053
Max., min. electron density/e Å^{-3}	2.10, −0.84	0.38, −0.37	0.32, −0.36

small and poorly formed crystal of $[Ni(HL^1_H)]Cl$ was weak, especially at higher angles; significant residual electron density is found close to the Ni atom in this structure, and the R values are relatively high, but the refinement is otherwise satisfactory. Programs used were standard data collection and processing software, *SHELXTL* and *SHELXL*-2013.[17]

Kinetics studies

All kinetic studies were conducted using an Applied Photophysics SX.18MV stopped-flow spectrophotometer. The temperature was maintained at 25.0 ± 0.1 °C using a Grant LTD6G recirculating thermostated tank. All solutions were prepared in air and were transferred into the stopped-flow spectrophotometer using all-glass syringes. The solutions of $NiCl_2{\cdot}6H_2O$ and the various Schiff base ligands were prepared from fresh stock solutions and used within 2 hours.

All kinetic studies were performed in methanol, with the concentration of Ni^{2+} = 0.2 or 0.5 mmol dm^{-3}. Because of limited solubility, the concentrations of the salicaldimine-based ligands were in the range 1–4 mmol dm^{-3}. The reactions of Ni^{2+} with the various Schiff base ligands were studied at λ = 460 nm. At this wavelength there is an increase in absorbance, as shown in Fig. 5 (insert). The reactions of Ni^{2+} with L_{py}, L^n_{py} and $H_2L^n_H$ (n = 1–3) were studied under pseudo first order conditions. However, the reactions with $H_2L^a_X$, H_2L_X–Cl, $H_2L^0_X$ and H_2salphen were all studied using concentrations which are not strict pseudo first-order conditions so the suitability of exponential curve fits to the data needs to be justified. There are three lines of evidence which validate the use of exponential fits for the reactions with $H_2L^a_X$, H_2L_X–Cl, $H_2L^0_X$ and H_2salphen. (1) For the reactions of $H_2L^a_H$, H_2L_X–Cl (X = H or Me), $H_2L^0_X$ (X = H, MeO, Me or Cl) and H_2salphen the traces were good fits to single exponential curves at all concentrations (examples shown in ESI†). (2) For $H_2L^a_X$ (X = Me or Cl), H_2L_{Cl}–Cl, and

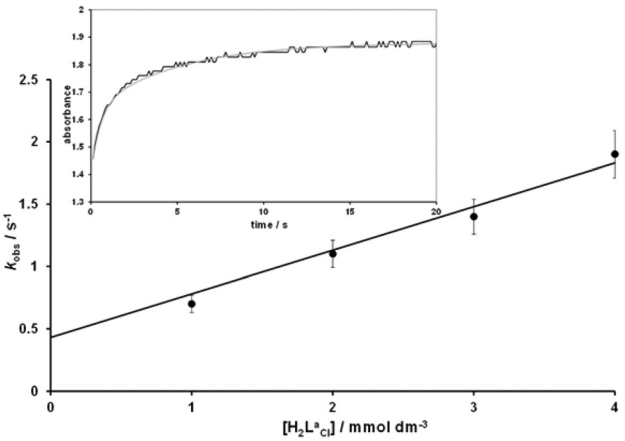

Fig. 5 (Main) Plot of k_{obs} *versus* concentration of $H_2L^a_{Cl}$ for the first phase of the reaction between $H_2L^a_{Cl}$ and Ni^{2+} in methanol at 25.0 °C. (Insert) Stopped-flow absorbance–time trace (black curve) for the reaction of $H_2L^a_{Cl}$ (4 mmol dm^{-3}) with Ni^{2+} (0.5 mmol dm^{-3}) in methanol at 25.0 °C, λ = 460 nm. The curve is fitted to the expression A_t = 1.90 − 0.24e$^{-1.93t}$ − 0.24e$^{-0.22t}$ (grey curve).

$H_2L^n_H$ (n = 1–3), the absorbance–time traces could be fitted to two exponentials. Analysis of the same data applying second order kinetics[18] also showed biphasic behaviour with rate constants for both phases in good agreement with those derived using exponential curve fits (examples shown in ESI†). (3) In selected studies with $[Ni^{2+}]$ = 0.2 mmol dm^{-3} and [ligand] = 2–4 mmol dm^{-3} (where [ligand]/$[Ni^{2+}] \geq 10$) the exponential curve fits gave observed rate constants in good agreement with those determined when $[Ni^{2+}]$ = 0.5 mmol dm^{-3} (ESI†). These observations indicate it is appropriate to fit the absorbance–time traces with exponential curves to obtain the observed first-order rate constants (k_{obs}). In the reactions with $H_2L^a_X$, H_2L_X–Cl, $H_2L^n_X$ and H_2salphen, both the absorbance change

and the final absorbance increase with increasing concentration of the ligand. This is a consequence of both the ligand absorbing at λ = 460 nm and the binding of these ligands to Ni^{2+} being equilibrium reactions. For the reactions with L_{py} and L^n_{py}, the absorbance change is independent of the concentration of ligand, but the final absorbance increases with increase in the concentration of ligand. This behaviour is because the ligands absorbs at λ = 460 nm but binding of L_{py} or L^n_{py} to Ni^{2+} are not equilibrium reactions (spectroscopic changes are presented in ESI†). That the binding of Ni^{2+} to $H_2L^a_X$, H_2L_X–Cl, $H_2L^0_X$ and H_2salphen are equilibrium reactions suggests the reason why the absorbance–time curves are good fits to exponential curves. In equilibrium reactions, the concentrations of Ni^{2+} and ligand that are added to the solution are not good indicators of the concentrations which are reacting. Using the values of the equilibrium constants for the reactions, $K_a = k_a/k_{-a}$, derived from the kinetic studies (Table 5), we have calculated for solutions where added concentrations are [ligand] = 1 mmol dm^{-3}, [Ni^{2+}] = 0.5 mmol dm^{-3}, that the concentration of ligand is 4–40 times larger than the 'reacting concentration' of Ni^{2+} (ESI†).

The dependences of k_{obs} on the concentrations of the ligands were determined from plots of k_{obs} *versus* concentration of Schiff base. For $H_2L^a_H$, H_2L_H–Cl, H_2L_{Me}–Cl, $H_2L^0_X$ and H_2salphen (traces fit single exponentials), such plots were straight line graphs with a positive intercept, as shown by the example in Fig. 5 (main). For the reactions with $H_2L^a_{Me}$, $H_2L^a_{Cl}$, H_2L_{Cl}–Cl and $H_2L^n_H$ (traces fit two exponentials), the values of k_{obs}, for the fast phase, also showed a linear dependence on the concentration of ligand with a positive intercept. For the slow phase, the values of k_{obs} were independent of the concentration of ligand. The values of k_{obs} presented in Tables 5 and 6 are the average of at least three duplicate experiments where the values of k_{obs} all agree within 10%, and this is reflected in the error bars presented in Fig. 5 and 10.

Results and discussion

Products of the reactions of the ligands with Ni^{2+}

Not all the products from the reactions of Ni^{2+} with the various ligands shown in Fig. 2 have been isolated. Those that have been isolated show the structure of the product depends on the composition of the ligand.

The structure of [$Ni(L^0_H)$] (*i.e.* [Ni(salen)]) has been known for some time and is square planar with both oxygen and both nitrogen donors coordinated.[21] The complexes NiL^a_H, NiL^a_{Me}, NiL^a_{Cl} have previously been characterized by spectroscopic techniques. All of the $H_2L^a_X$ are potential N_2O_2-type quadridentate ligands and the room-temperature magnetic properties of the reaction products of $H_2L^a_H$ and $H_2L^a_{Cl}$ with Ni^{II} salts indicate the complexes are binuclear with Ni–Ni interactions.[11] The dimeric nature of these complexes was further indicated by mass spectrometry, where the molecular ion was observed at the position corresponding to a dimer. On the other hand, the analysis for the $H_2L^a_{Me}$ product indicates it is mononuclear.[12]

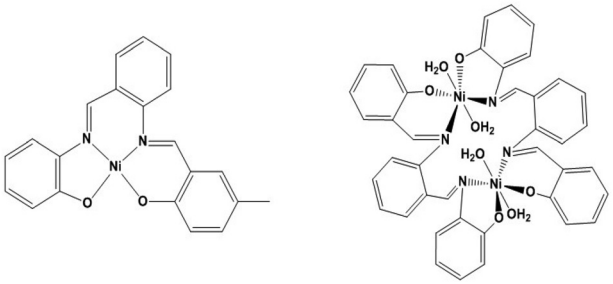

Fig. 6 Suggested structures of Ni complexes, NiL^a_{Me} (left hand side) and $Ni_2(L^a_X)_2$ (X = H or Cl) (right hand side).

Suggested structures of the complexes NiL^a_H, NiL^a_{Me} and NiL^a_{Cl} are shown in Fig. 6.

The further diversity of the structures of the products of the reactions between Ni^{2+} and the multidentate ligands is illustrated by the X-ray crystal structures for which the cations are shown in Fig. 7; selected bond lengths and angles describing the metal coordination geometry are given in Table 4. Although $H_2L^1_H$, L^1_{py} and L_{py} all have five potential donor atoms, only with L_{py} do all donor atoms bind to a single Ni. With $H_2L^1_H$, and L^1_{py} the inflexibility of the ligand results in a dimeric structure ([{$NiCl(L^1_{py})$}$_2$]Cl_2) or a mononuclear species with a pendant arm ([$Ni(HL^1_H)$]Cl). The product with L_{py} is a mononuclear complex containing an octahedral Ni in [$Ni(L_{py})Cl]^+$, which is coordinated by the five donor nitrogens of L_{py} and a chloro ligand. In contrast, the Ni complex with L^1_{py} is a dimeric dication {[$Ni_2(L^1_{py})_2Cl_2]^{2+}$}. The coordination sphere of each Ni is identical. Each Ni is octahedral, with one L^1_{py} acting as a tridentate ligand and the other acting as a bidentate. The final coordination site on each Ni is occupied by a chloro ligand. It is impossible for all five nitrogen donors in L^1_{py} to coordinate to a single octahedral Ni because it is only the central NH group which is capable of subtending two chelate arms which are 90° to one another. $H_2L^1_H$ is also too inflexible to be pentadentate to a single Ni. However, in this case, the geometry at the Ni is square planar. The four donors to the Ni are one oxygen of a phenolate residue, the two imine nitrogens and the NH group. The remaining phenol residue is uncoordinated and remains protonated.

All the structures are of chloride salts. Two of them are solvates, both containing methanol and one of them also water. The solvent molecules and chloride anions are involved in hydrogen bonding, with most N–H groups of the ligands also acting as donors. Full details available in ESI.†

We have isolated the products of the reactions of Ni^{2+} with L^1_H, L^2_H or L^3_H. Attempts to determine the X-ray crystal structures for the products of Ni^{2+} with L^2_H and L^3_H were unsuccessful, but the ^{1}H NMR spectra of the isolated compounds (ESI†) show sharp resonances in similar positions to those for [$Ni(HL^1_H)]^+$ indicating that in these systems similar square-planar complexes are formed, presumably with pendant groups. However, the ^{1}H NMR spectra also show some broad resonances (particularly for the product with L^3_H), indicating paramagnetic products (either octahedral or tetrahedral) are also present, possibly in equilibrium. It is worth noting that the kinetics of

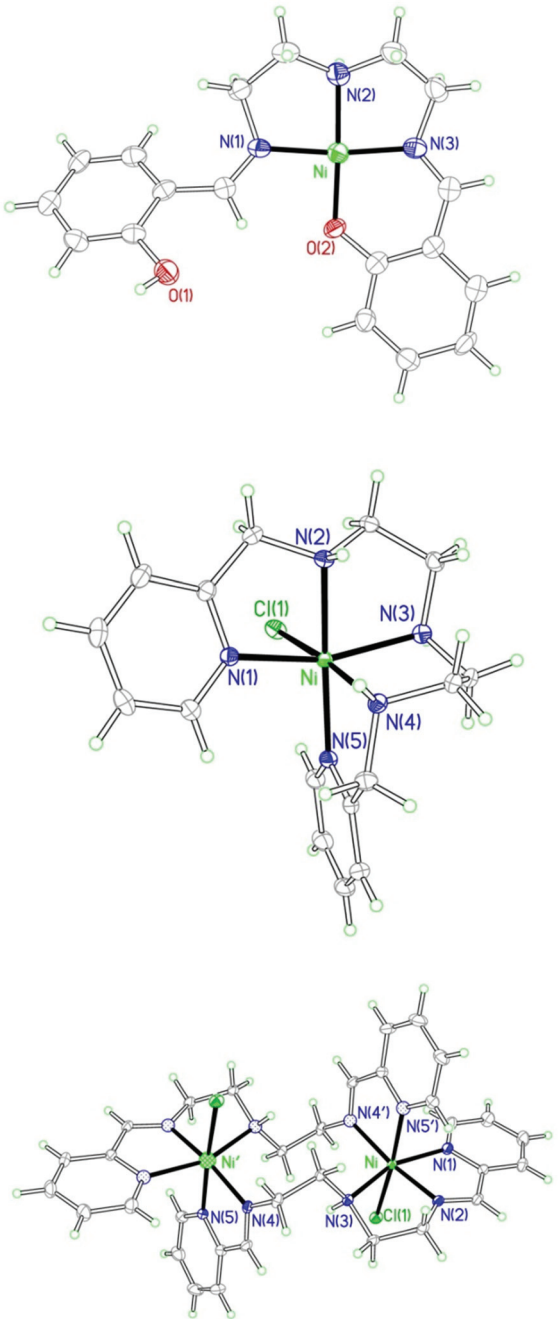

Fig. 7 Crystallographically determined structures of the cations $[Ni(HL^1_H)]^+$, $[NiCl(L_{py})]^+$ and $[\{NiCl(L^1_{py})\}_2]^{2+}$. Displacement ellipsoids are shown at the 40% probability level, and selected atoms are labelled; primes indicate atoms generated by inversion symmetry in the centrosymmetric dimeric cation.

Table 4 Selected bond lengths (Å) and angles (°) at the Ni atoms in $[Ni(HL^1_H)]^+$, $[NiCl(L_{py})]^+$ and $[\{NiCl(L^1_{py})\}_2]^{2+}$

$[Ni(HL^1_H)]^+$ (pendant arm)			
Ni–N(1)	1.891(6)	N(1)–Ni–N(2)	86.2(3)
Ni–N(2)	1.883(6)	N(1)–Ni–O(2)	91.6(2)
Ni–N(3)	1.837(6)	N(2)–Ni–N(3)	86.4(3)
Ni–O(2)	1.823(4)	N(3)–Ni–O(2)	96.0(2)
		N(1)–Ni–N(3)	171.4(3)
		N(2)–Ni–O(2)	177.3(2)
$[NiCl(L_{py})]^+$ (mononuclear)			
Ni–Cl(1)	2.4634(6)	Cl(1)–Ni–N(1)	91.73(5)
Ni–N(1)	2.0948(17)	Cl(1)–Ni–N(2)	91.26(5)
Ni–N(2)	2.0714(18)	Cl(1)–Ni–N(3)	95.06(5)
Ni–N(3)	2.1181(19)	Cl(1)–Ni–N(4)	171.51(5)
Ni–N(4)	2.1277(18)	Cl(1)–Ni–N(5)	91.82(5)
Ni–N(5)	2.0956(17)	N(1)–Ni–N(2)	79.23(7)
		N(1)–Ni–N(3)	160.01(7)
		N(1)–Ni–N(4)	92.56(7)
		N(1)–Ni–N(5)	100.96(7)
		N(2)–Ni–N(3)	81.85(7)
		N(2)–Ni–N(4)	96.74(7)
		N(2)–Ni–N(5)	176.91(7)
		N(3)–Ni–N(4)	83.31(7)
		N(3)–Ni–N(5)	97.60(7)
		N(4)–Ni–N(5)	80.17(7)
$[\{NiCl(L^1_{py})\}_2]^{2+}$ (dimeric)			
Ni–Cl(1)	2.4222(4)	Cl(1)–Ni–N(1)	90.02(3)
Ni–N(1)	2.1014(11)	Cl(1)–Ni–N(2)	94.64(3)
Ni–N(2)	2.0020(11)	Cl(1)–Ni–N(3)	85.76(3)
Ni–N(3)	2.1293(11)	Cl(1)–Ni–N(4′)	94.25(3)
Ni–N(4′)	2.0726(11)	Cl(1)–Ni–N(5′)	172.57(3)
Ni–N(5′)	2.1226(11)	N(1)–Ni–N(2)	78.62(4)
		N(1)–Ni–N(3)	159.78(4)
		N(1)–Ni–N(4′)	99.77(4)
		N(1)–Ni–N(5′)	89.03(4)
		N(2)–Ni–N(3)	82.02(4)
		N(2)–Ni–N(4′)	170.96(4)
		N(2)–Ni–N(5′)	92.39(4)
		N(3)–Ni–N(4′)	100.26(4)
		N(3)–Ni–N(5′)	97.60(4)
		N(4′)–Ni–N(5′)	78.66(5)

the reactions between all the ligands and Ni^{2+} do not reflect the composition (nuclearity) of the product.

Kinetics of the reactions of Ni^{2+} with $H_2L^a_X$, H_2L_X–Cl, H_2salphen or $H_2L^0_X$

The kinetics of the reactions between Ni^{2+} and $H_2L^a_X$, H_2L_X–Cl, H_2salphen or $H_2L^0_X$ have been studied in methanol. Both the spectroscopic changes and the kinetics of these reactions (Experimental section) indicate that binding of these ligands are equilibrium reactions. Furthermore, the reactions of $H_2L^a_X$ (X = Me or Cl), and H_2L_{Cl}–Cl with Ni^{2+} are associated with two phases in which the second phase occurs at a rate independent of the concentration of ligand. For the reactions of $H_2L^a_H$, H_2L_X–Cl (X = H or Me), H_2salphen and $H_2L^0_X$ (X = H, Me, MeO or Cl), and the fast phase of the reactions with $H_2L^a_X$ (X = Me or Cl) and H_2L_{Cl}–Cl the rate law is that shown in eqn (1). The rate law associated with the second phase of the reactions with $H_2L^a_X$ (X = Me or Cl) and H_2L_{Cl}–Cl is shown in eqn (2). The values of k_a, k_{-a} and k_b are summarised in Table 5. For the reactions of all the ligands presented in Table 5, k_a is the rate constant for the binding and k_{-a} is the rate constant for the dissociation of the ligand with Ni^{2+}.

$$\text{Rate} = \{k_{-a} + k_a[\text{ligand}]\}[Ni^{2+}] \quad (1)$$

$$\text{Rate} = k_b[Ni^{2+}] \quad (2)$$

Table 5 Summary of the rate constants in the reactions between Ni^{2+} and Schiff base ligands measured in methanol at 25.0 °C

Ligand	k_{-a}/s^{-1}	$k_a/dm^3\ mol^{-1}\ s^{-1}$	k_b/s^{-1}
Unsymmetrical Schiff bases			
$H_2L^a_H$	0.022 ± 0.005	19.0 ± 1.0	—
$H_2L^a_{Me}$	0.35 ± 0.02	87.5 ± 10	0.06 ± 0.01
$H_2L^a_{Cl}$	0.43 ± 0.02	350 ± 30	0.20 ± 0.05
H_2L_H–Cl	0.11 ± 0.02	5.0 ± 0.3	—
H_2L_{Me}–Cl	0.013 ± 0.005	19.3 ± 1.0	—
H_2L_{Cl}–Cl	0.22 ± 0.02	32.5 ± 2.0	0.04 ± 0.01
Symmetrical Schiff bases			
$H_2L^0_H$	0.022 ± 0.005	6.5 ± 0.5	—
$H_2L^0_{OMe}$	0.014 ± 0.005	5.5 ± 0.5	—
$H_2L^0_{Me}$	0.018 ± 0.005	2.0 ± 0.2	—
$H_2L^0_{Cl}$	0.013 ± 0.005	12.0 ± 1.0	—
H_2salphen	0.010 ± 0.005	4.0 ± 0.5	—

Comparison of the reactivities of Ni^{2+} with $H_2L^a_X$, H_2L_X–Cl, H_2salphen or $H_2L^0_X$

It is not clear if the observed reversible reactions for the ligands in Table 5 correspond to the complete attachment of the ligand to the metal, or just partial attachment. Although all the ligands are quadridentates, in no case do we observe a four-step time course. The rate constants presented in Table 5 relate to the first phase, or first and second phases of the wrapping. However, from these kinetics alone, it is not possible to establish if the first phase {eqn (1)} corresponds to the binding of the first donor of the ligand or to the first chelation of the ligand (*vide infra*). The second phase {eqn (2)} is independent of the concentrations of the ligands and this is consistent with an intramolecular chelation of the partially coordinated ligand. There are several possible reasons why two phases are observed in some reactions, but only one phase in others. It could be that for some systems the second phase is too slow to be observed over the time-scale of the stopped-flow experiments (*ca.* 100 s). Alternatively, it could be that for some ligands the second phase is faster than the first phase. Finally, it could be that, in some systems, the absorbance change of the second phase is too small to be detectable.

The kinetics observed for the reactions of Ni^{2+} with $H_2L^0_X$, H_2salphen, $H_2L^a_X$ and H_2L_X–Cl are consistent with the mechanism shown in the top line of Fig. 8. This is the Eigen–Wilkins mechanism[22–24] which involves an initial outer-sphere association between the multidentate ligand and Ni^{2+} (K_L), followed by the dissociation of a coordinated solvent molecule from Ni^{2+} (k_2), and the subsequent binding of the first donor atom of the multidentate. Extensive studies have shown that in the reactions with Ni^{2+}, the dissociation of the coordinated solvent occurs at a rate essentially independent of the nature of the nucleophile.[25] Depending on the multidentate ligand, the rate-limiting step for the reaction can either be the formation of **A** {rate law shown in eqn (3), assuming $K_L[L] < 1$} or the formation of **B** {rate law shown in eqn (4), assuming $K_L[L] < 1$}. Clearly, the kinetics cannot distinguish between the rate-limiting step being the initial binding of the multidentate to Ni^{2+} or the subsequent chelation step.

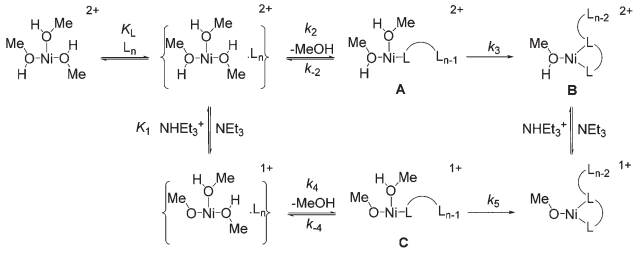

Fig. 8 The mechanism for the reactions of multidentate ligands with Ni^{2+} in methanol (top line). Also included is the conjugate base pathway (bottom line) observed in the presence of mixtures of $NHEt_3^+$ and NEt_3.

$$\text{Rate} = K_L k_2 [L][Ni^{2+}] \quad (3)$$

$$\text{Rate} = \frac{K_L k_2 k_3 [L][Ni^{2+}]}{k_{-2} + k_3} \quad (4)$$

The kinetic data presented in Table 5 relate to the reactions of both conventional, symmetric types ($H_2L^0_X$ and H_2salphen) and asymmetric types ($H_2L^a_X$ and H_2L_X–Cl) salicaldimine-based quadridentate ligands. The values of the rate constants {k_{-a} = 0.01–0.43 s^{-1}, k_a = 4.0–350 $dm^3\ mol^{-1}\ s^{-1}$ and k_b = 0.04–0.20 s^{-1}} shows that there is not a large variation in any of the rate constants. Furthermore, the values of k_a and k_{-a} are very similar to the rate constants observed in many other kinetic studies on the binding of various N, O or F donor ligands to Ni^{2+}.[24] Thus, changes of the bridging residue (CH_2CH_2, C_6H_4 or anthracene), the symmetry of the imine bonds and the substituent (on the phenolic residue) have little effect on k_a, k_{-a} or k_b. The minor differences observed in k_a are presumably attributable to slight variations in K_L. The similar reactivities of $H_2L^0_X$, H_2salphen, $H_2L^a_X$ and H_2L_X–Cl (Table 5), and particularly that electron-withdrawing and electron-donating substituents on the phenolic group have similar effects on the reactivity, indicates that the outer-sphere association (K_L) is rather non-specific.

Kinetic studies on the reactions of Ni^{2+} with $H_2L^n_H$ and L^n_{py} (n = 0–3)

In a further series of studies, the kinetics of the reactions between Ni^{2+} and $H_2L^n_H$ (n = 1–3) have been investigated. The $H_2L^n_H$ ligands have features in common with the Schiff base ligands presented in Table 5 (*i.e.* neutral ligands with terminal salicaldimine residues). However, in $H_2L^n_H$, a number of NH groups are introduced into the ligand.

The reactions of all $H_2L^n_H$ (n = 1–3) with Ni^{2+} in methanol are associated with two phases with the rate law for the first phase being that presented in eqn (1) and the rate law for the second phase being that shown in eqn (2). The rate constants for these reactions are summarised in Table 6 and Fig. 9. It is clear that the presence of the NH groups results in significantly faster rates ($k_a \geq 1 \times 10^3$ $dm^3\ mol^{-1}\ s^{-1}$). Indeed, these rates are similar to, or faster than, the solvent exchange rate for $[Ni(MeOH)_6]^{2+}$ which is in the range $k = 2 \times 10^2$–1×10^3 s^{-1}.[26] Similar behaviour has been observed (in aqueous

Table 6 Summary of the rate constants in the reactions between Ni^{2+} and $H_2L^n_H$ measured in methanol at 25.0 °C

Ligand	n^a	k_{-a} /s^{-1}	k_a/dm^3 mol^{-1} s^{-1}	k_b/s^{-1}
Symmetrical Schiff bases				
$H_2L^0_H$	0	0.022 ± 0.005	6.5 ± 0.5	—
$H_2L^1_H$	1	0.35 ± 0.02	1.0 ± 0.1 × 10^3	0.04 ± 0.01
$H_2L^2_H$	2	1.1 ± 0.1	1.1 ± 0.1 × 10^3	0.05 ± 0.01
$H_2L^3_H$	3	2.0 ± 0.2	1.3 ± 0.1 × 10^3	0.01 ± 0.005
Pyridyl Schiff bases				
L^0_{py}	0		3.2 ± 0.3 × 10^3	
L^1_{py}	1		4.3 ± 0.3 × 10^3	
L^2_{py}	2		4.8 ± 0.3 × 10^3	
L^3_{py}	3		5.3 ± 0.3 × 10^3	
Pyridyl pentadentate				
L_{py}	3		0.8 ± 0.1 × 10^3	

[a] n = number of NH groups.

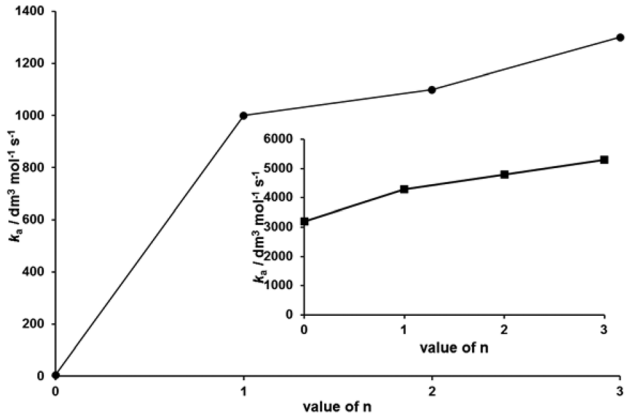

Fig. 9 (Main) Variation of rate of reaction between Ni^{2+} and $H_2L^n_H$ (n = 0–3). The data presented are for the formation pathway {k_a in eqn (1)}. A similar trend is observed for the corresponding dissociation pathway {k_{-a} in eqn (1)}. (Insert) Variation of rate of reaction between Ni^{2+} and L^npy (n = 0–3).

solution) for the reactions between $[Ni(OH_2)_6]^{2+}$ and aliphatic polyamines.[27] It has been suggested, in these earlier studies, that a so-called 'internal conjugate base mechanism' could operate in these systems. The internal conjugate base mechanism involves hydrogen bonding of a coordinated MeOH to an NH group in the outer-sphere association between the ligand and Ni^{2+}. This hydrogen bonding imparts methoxide character to the methanol ligand which labilises the other Ni-methanol co-ligands (*vide infra*).

A further feature of the reactivities of $H_2L^n_H$ is evident in Fig. 9. It is clear that the rate of the reactions increase with the value of n. However, whilst there is a large increase in rate between $H_2L^0_H$ and $H_2L^1_H$, the subsequent increases in the rates for $H_2L^2_H$ and $H_2L^3_H$ are much smaller. The large difference in rates between $H_2L^0_H$ and $H_2L^1_H$ indicates that even a single NH group leads to a significant increase in the rate. The smaller increases in rate associated with $H_2L^2_H$ and $H_2L^3_H$ are a consequence of the increase in the number of potential NH donor atoms (statistical effect). Consistent with this interpretation, earlier studies on the reactions of Ni^{2+} with $(NH_2CH_2CH_2NHCH_2)_2$ or $(NH_2CH_2CH_2NHCH_2CH_2)_2NH$ in the presence of acid showed that the rates of the reactions with the various protonated forms of these ligands are dominated by an electrostatic effect, but statistical factors also contribute.[27,28]

Studies on another series of ligands show a similar behaviour to that of $H_2L^n_H$. The L^n_{py} ligands are structurally similar to $H_2L^n_H$ but contain terminal pyridyl residues rather than phenolic groups. For the reactions between Ni^{2+} and L^n_{py}, both the spectrophotometric changes and the kinetics indicate that these reactions go essentially to completion (Experimental section). The associated rate law for the reactions is eqn (5).

$$\text{Rate} = k_a[L^n_{py}][Ni^{2+}] \quad (5)$$

The values of k_a are presented in Table 6 and Fig. 9 (insert). Two aspects of these data are worthy of comment. First, comparison of the data for the analogous ligands $H_2L^0_H$ and L^0_{py} shows that L^0_{py} reacts nearly 10^3 times faster than $H_2L^0_H$, indicating that a pyridyl residue, like an NH group, is a labilising influence in these reactions. Secondly, it is evident from the data for L^n_{py} that the rate of the reaction increases as the number of NH groups increase, in a similar fashion to that observed for $H_2L^n_H$. The rate of the reaction of Ni^{2+} with the saturated quinquidentate ligand, L_{py} also occurs at a rate similar to those observed for L^n_{py}. Finally, it is worth noting that both L_{py} and L^1_{py} have the same number, but different types, of N donors. Comparison of the rates of the reactions of Ni^{2+} with these two ligands indicates that the imine N has a minor or negligible effect on the rate of binding.

That ligands containing either, or both, pyridyl and NH groups result in fast reactions with Ni^{2+} requires further consideration. The increased rate of reaction (faster than that of the solvent exchange rate for $[Ni(MeOH)_6]^{2+}$) could be either due to both pyridyl and NH groups being involved in 'internal conjugate base mechanisms' or that the reactions being observed involve rate-limiting chelate formation with the rate of chelation being rapid because initial coordination of a pyridyl or NH group affects the lability of the coordinated methanol. To further address this issue we have studied the effect of deprotonating a coordinated methanol (by a non-coordinating base, NEt_3) has on the rate of reactions between Ni^{2+} and $H_2L^0_H$.

Effect of NEt_3 on the reactions between Ni^{2+} and $H_2L^0_H$: the conjugate base mechanism

The rate of the reaction between Ni^{2+} and $H_2L^0_H$ is affected by the ratio $[NHEt_3^+]/[NEt_3]$ as shown in Fig. 10. At high $[NHEt_3^+]/[NEt_3]$ the rate of the reaction is essentially that observed in the studies between Ni^{2+} and $H_2L^0_H$ described earlier in this paper. However, at low $[NHEt_3^+]/[NEt_3]$ the rate increases and the absorbance–time curves become biphasic with k^1_{obs} for the fast phase dependent on $[NHEt_3^+]/[NEt_3]$ and the slow phase independent of $[NHEt_3^+]/[NEt_3]$ (k^2_{obs} = 21.0 ± 2.0 s^{-1}). The

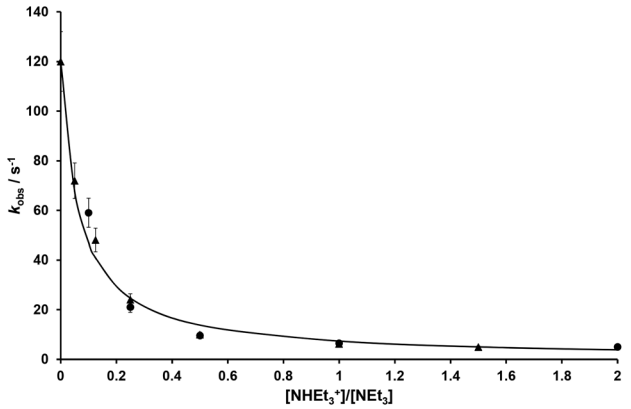

Fig. 10 Dependence of k_{obs} on the ratio $[NHEt_3^+]/[NEt_3]$ for the reaction of $H_2L^0_H$ (2.5 mmol dm^{-3}) with Ni^{2+} (0.5 mmol dm^{-3}) in MeOH at 25.0 °C. Data points correspond to $[NEt_3]$ = 20 mmol dm^{-3}, $[NHEt_3^+]$ = 0–30 mmol dm^{-3} (▲); $[NEt_3]$ = 10 mmol dm^{-3}, $[NHEt_3^+]$ = 0–30 mmol dm^{-3} (●). Curve drawn is that defined by eqn (6).

increase in k^1_{obs} at low $[NHEt_3^+]/[NEt_3]$ indicates a deprotonation is labilising. We presume that at all values of $[NHEt_3^+]/[NEt_3]$ the reaction also exhibits a first order dependence on the concentration of $H_2L^0_X$. We have shown that when $[NHEt_3^+]/[NEt_3]$ = 2, the reaction does indeed exhibit a first order dependence on the concentration of $H_2L^0_H$ (ESI†). However, it is difficult to demonstrate a similar dependence on the concentration of $H_2L^0_H$ at low $[NHEt_3^+]/[NEt_3]$ because the rate of reaction, under these conditions, is close to the limit of the stopped-flow apparatus. Analysis of the data shown in Fig. 10 yields the rate law shown in eqn (6), when $[H_2L^0_H]$ = 2.5 mmol dm^{-3}.

$$\text{Rate} = \frac{\{120 + 0.23[NHEt_3^+]/[NEt_3]\}[Ni^{2+}]}{1 + 15.5[NHEt_3^+]/[NEt_3]} \quad (6)$$

$$\text{Rate} = \frac{\{K_L k_d + (K_L k_c/K_1)[NHEt_3^+]/[NEt_3]\}[H_2L^0_H][Ni^{2+}]}{1 + (1/K_1)[NHEt_3^+]/[NEt_3]} \quad (7)$$

The data in Fig. 10 shows that k_{obs} depends on the ratio $[NHEt_3^+]/[NEt_3]$, but not the absolute concentrations of either of these reactants. This behaviour indicates that only a single deprotonation occurs. There are two candidates for being deprotonated: either $[Ni(MeOH)_6]^{2+}$ or $H_2L^0_H$. In methanol, the pK_a of $NHEt_3^+$ is 10.7[29] and the pK_a of phenol is 14.3,[30] and so, over the range of $[NHEt_3^+]/[NEt_3]$ used in these studies essentially all $H_2L^0_H$ remains diprotonated. Thus the dependence on $[NHEt_3^+]/[NEt_3]$ must be attributable to the formation of the conjugate base, $[Ni(OMe)(MeOH)_5]^+$.

The mechanism consistent with the kinetics in the presence of $[NHEt_3^+]/[NEt_3]$, is presented in Fig. 8. The top line of Fig. 8 presents the pathway described earlier (observed in the absence of base), whilst the lower pathway is the conjugate base mechanism. In this lower pathway, rapid deprotonation of a coordinated methanol produces $[Ni(OMe)(MeOH)_5]^+$ (K_1), which reacts more rapidly with $H_2L^0_H$, presumably because $[Ni(OMe)(MeOH)_5]^+$ is more labile to methanol dissociation than $[Ni(MeOH)_6]^{2+}$.[31]

The rate law associated with the mechanism shown in Fig. 8 is presented in eqn (7), where $k_c = k_2$ (if binding of the first donor is rate-limiting) or $k_c = k_2k_3/(k_{-2} + k_3)$ (if chelation is rate-limiting) and $k_d = k_4$ (if binding of the first donor is rate-limiting) or $k_d = k_4k_5/(k_{-4} + k_5)$ (if chelation is rate-limiting). Eqn (7) is derived assuming that both K_L and K_1 are rapidly established equilibria and that both species **A** and **C** (in Fig. 8) are steady state intermediates. Comparison of eqn (6) and (7) yields the values K_Lk_c = 6.0 ± 0.5 dm^3 mol^{-1} s^{-1}, K_Lk_d = (4.8 ± 0.5) × 10^4 dm^3 mol^{-1} s^{-1} and K_1 = 0.065 ± 0.01. Consideration of these kinetic parameters for the reactions between Ni^{2+} and $H_2L^0_H$ in the presence of mixtures of NEt_3 and $NHEt_3^+$ allow us to calculate pK_a = 11.9 ± 0.1 for $[Ni(MeOH)_6]^{2+}$. This value is reasonable, because previous studies have shown that pK_a = 9.2–10.9 for $[Ni(OH_2)_6]^{2+}$.[32] Using the relationship, pK_a(MeOH) = 1.02pK_a(H_2O) + 0.72,[33] we can estimate pK_a = 10.1–11.8 for $[Ni(MeOH)_6]^{2+}$, in good agreement with that measured in these studies. Furthermore, the ratio $k_d/k_c = (8.0 \pm 1.1) \times 10^3$ is a measure of the increased lability of $[Ni(OMe)(MeOH)_5]^+$ compared to $[Ni(MeOH)_6]^{2+}$. The best fit value for K_Lk_c = 6.0 ± 0.5 dm^3 mol^{-1} s^{-1}, derived from this analysis, is in reasonable agreement with the value $K_Lk_c = k_a$ = 6.5 ± 0.5 dm^3 mol^{-1} s^{-1} measured directly for the reaction of Ni^{2+} with $H_2L^0_H$ (Table 5).

The slow phase only becomes evident when $k^1_{obs} \geq$ *ca.* 50 s^{-1}. It seems likely that the slower phase, k^2_{obs} = 21.0 ± 2.0 s^{-1}, corresponds to the chelation step and becomes distinct only when $k^1_{obs} > k^2_{obs}$.

Kinetics of binding and evidence of preferential binding

The results from the kinetic studies of the reactions between Ni^{2+} and $H_2L^0_X$ in the presence of mixtures of NEt_3 and $NHEt_3^+$ allow us to make some conclusions concerning: (i) the involvement of an internal conjugate base mechanism in the reactions with ligands containing pyridyl or NH groups and (ii) the preferential binding of certain groups to Ni^{2+}.

The increased rates observed in the reactions with $H_2L^n_X$ and L^n_{py} are consistent with an 'internal conjugate base mechanism' involving the NH groups (pK_a ~ 11).[30] However, it seems unreasonable that the increase in rate observed between $H_2L^0_H$ and L^0_{py} is due to the pyridyl groups operating an 'internal conjugate base mechanism' because the pyridyl group is a much weaker base (pK_a ~ 5).[30] It seems more likely that the enhanced rate observed with L^0_{py} is consistent with the mechanism shown in Fig. 8, where chelation is the rate-limiting step. Thus, the increased reactivity observed with L^0_{py} is attributable to the initial coordination of the pyridyl group to the Ni and the presence of the pyridyl group in the coordination sphere of the Ni labilises the methanol co-ligands hence facilitating the chelation step (k_3).

Conclusions

The aim of this work was to see if kinetics (specifically the rates of reactions) could be used to probe which donor site in a multidentate ligand binds preferentially to a metal ion. The

kinetic studies reported herein for the reactions of Ni^{2+} with a variety of similar neutral multidentate ligands containing various types of donors (phenolic OH, imine N, pyridyl N and NH) certainly indicate that the rates of reactions depend on the composition of the ligands, and follows the order: NH > pyridyl N > phenolic OH ~ imine N. However, only with ligands containing pyridyl groups is there evidence that this order reflects preferential initial binding of specific groups to Ni^{2+}. The rapid reactions observed with ligands containing NH groups could also be due to preferential initial binding of the NH group to Ni^{2+}, but the NH groups are sufficiently basic to possibly be involved in an 'internal conjugate base mechanism', and this could be the origin of the increased reactivity observed with ligands containing NH groups.

Studies on ligands containing terminal phenolic groups ($H_2L^0_X$, $H_2L^a_X$, H_2L_X–Cl) show that the rates of reactions are all similar, and rather insensitive to substituents on the phenolic groups, symmetry of the imine bonds and nature of bridge between phenolic groups. This indicates that for $H_2L^0_X$, $H_2L^a_X$, H_2L_X–Cl that either the binding of the first donor is rate-limiting (k_2) or, that if chelation (k_3) is rate-limiting, the binding of the first donor to Ni has little effect on the lability of the methanol co-ligands.

In the long term it is anticipated that understanding the preferences of different donors binding to metal ions will contribute to understanding the dynamics of metal ions being encapsulated by biomolecules. In this study we deliberately chose to study reactions with Ni^{2+}, where the substitution mechanism is predominantly dissociative. Future studies will explore the reactions of multidentate ligands with metal ions where associative substitution mechanisms can operate.

Acknowledgements

We thank Mr Thaer Al-Rammahi and Dr Ahmed Al-Saffar for assistance with some experiments. This work is supported by the Council of Higher Education (Turkey) and the Research Foundation of Nevşehir University (BAP 2010/17). We thank EPSRC (UK) for equipment funding.

Notes and references

1 E. Horst, *Coord. Chem. Rev.*, 1999, **187**, 37, and references therein.
2 R. G. Wilkins, *Comments Inorg. Chem.*, 1983, **2**, 187.
3 C. E. Castillo, M. A. Mánez, J. González, J. M. Llinares, H. R. Jiménez, M. G. Basallote and E. García-España, *Chem. Commun.*, 2010, **46**, 6081.
4 C. E. Castillo, J. González-García, J. M. Llinares, M. A. Máñez, H. R. Jimenez, E. García-España and M. G. Basallote, *Dalton Trans.*, 2013, **42**, 6131.
5 L. Siegfried, C. N. McMahon, J. Baumeister, M. Neuburger, T. A. Kaden, S. Anandaram and C. G. Palivan, *Dalton Trans.*, 2007, 4797.
6 J. Gonzalez, R. Gavara, O. Gadea, S. Blasco, E. Garcıa-Espana and F. Pina, *Chem. Commun.*, 2012, **48**, 1994.
7 (*a*) T. Punniyamurphy, S. Velusamy and J. Iqbal, *Chem. Rev.*, 2005, **105**, 2329; (*b*) E. N. Jacobsen, *Acc. Chem. Res.*, 2000, **33**, 421.
8 C. M. Da Silva, D. L. Da Silva, L. V. Modolo, R. B. Alves, M. A. De Resende, C. V. B. Martins and A. De Fatima, *J. Adv. Res.*, 2011, **2**, 1.
9 N. A. Negm and M. F. Zaki, *Colloids Surf., A*, 2008, **322**, 97.
10 Y.-F. Ji, R. Wang, S. Ding, C.-F. Du and Z.-L. Liu, *Inorg. Chem. Commun.*, 2012, **16**, 47.
11 D. Nartop, P. Gürkan, N. Sari and S. Çete, *J. Coord. Chem.*, 2008, **61**, 3516.
12 For both types of ligands (except for $H_2L^a_H$ and H_2L_{Cl}–Cl), these ligands are unsymmetrical in two senses: they are unsymmetrical with respect to the 'direction' of the imine bond (*i.e.* –CH=N-aryl-CH=N–) and they are unsymmetrical with respect to the substituents on the terminal phenolic residues. Throughout this paper, reference to unsymmetrical Schiff base ligands refers to the unsymmetrical nature of the imine bond.
13 Ö. Güngör and P. Gürkan, *Spectrochim. Acta, Part A*, 2010, **77**(1), 304.
14 H_2L_X–Cl show two strong bands in the region 1589–1624 cm^{-1}, attributable to $\nu_{C=N}$, and $\nu_{C=C}$ in the region 1454–1589 cm^{-1}.[19] Two bands are observed because of the two asymmetric imine groups. A similar characteristic has been reported for $H_2L^a_X$.[11] Because of the different chemical environments of the unsymmetrical imine groups, the ^1H NMR spectra of all H_2L_X–Cl show two signals in the range 8.31–8.97 ppm and 9.57–9.85 ppm (Table 2). The two phenolic protons of all H_2L_X–Cl are observed in the ranges 9.90–13.81 ppm. Finally, the peak attributable to CH_3 in H_2L_{Me}–Cl is observed at 2.50 ppm. The CH_3 group in H_2L_{Me} is also observed at 2.50 ppm.[20] The mass spectroscopy results for H_2L_X–Cl are presented in Table 1. The values of the molecular ion peaks and the fragmentation products are consistent with the proposed structures of unsymmetrical Schiff bases. The molecular ion peaks are observed at the predicted values of *m*/*z*: 399.2 $[M]^+$ (H_2L_H–Cl), 413.2 $[M - H]^+$ (H_2L_{Me}–Cl) and 433.0 $[M - 2H]^+$ (H_2L_{Cl}–Cl). The same fragmentation pathways appear for the highest intensity peaks in each ligand. Thus, peaks at *m*/*z* = 242.3, *m*/*z* = 262.1 and *m*/*z* = 282.0 for H_2L_H–Cl, H_2L_{Me}–Cl and H_2L_{Cl}–Cl, respectively, are attributed to the loss of the $[M - (C_7H_5NOCl) - 4H]^+$, $[M - (C_7H_5NOCl) + 2H]^+$, $[M - (C_7H_5NOCl) + 3H]^+$ fragments, which is common to all H_2L_X–Cl.
15 R. Pohloudek-Fabini and D. Froehling, *Arch. Pharm.*, 1965, **298**, 423.
16 M. Nakamura, K. Komatsu, Y. Gondo, H. Ohta and Y. Ueda, *Chem. Pharm. Bull.*, 1967, **15**, 585.
17 *SMART, SAINT and SADABS software*, Bruker AXS Inc., Madison, Wisconsin, USA, 2001; *CrysAlis Pro*, Agilent Technologies, Oxford, 2009; G. M. Sheldrick, *Acta Crystallogr., Sect. A: Fundam. Crystallogr.*, 2008, **64**, 112.

18 J. Espenson, *Chemical Kinetics and Reaction Mechanisms*, McGraw-Hill, New York, 1981, p. 16.
19 R. M. Silverstein, G. C. Bassler and T. C. Morrill, *Spectrophotometric Identification of Organic Compounds*, Wiley, New York, 1981.
20 E. Erdik, *Organik Kimyada Spektroskopik Yontemler*, Gazi Büro Kitapevi, Ankara, 1993, p. 201.
21 M. A. Siegler and M. Lutz, *Cryst. Growth Des.*, 2009, **9**, 1194, and references therein.
22 M. L. Tobe and J. Burgess, *Inorganic Reaction Mechanisms*, Longman, Harlow, 1999, p. 310.
23 R. G. Wilkins, *Kinetics and Mechanism of Reactions of Transition Metal Complexes*, VCH, Weinheim, 2nd edn, 1991, ch. 4.
24 J. Burgess, *Metal Ions in Solution*, Ellis Horwood, Chichester, 1978, ch. 10.
25 R. G. Wilkins, *Acc. Chem. Res.*, 1970, **3**, 409, and references therein.
26 H. P. Bennetto and E. F. Caldin, *J. Chem. Soc. A*, 1971, 2198.
27 (*a*) R. B. Jordan, *Reaction Mechanisms of Inorganic and Organometallic Systems*, OUP, New York, 1991, p. 84; (*b*) D. B. Rorabacher, *Inorg. Chem.*, 1966, **5**, 1891; (*c*) R. B. Jordan, *Inorg. Chem.*, 1976, **15**, 748.
28 D. W. Margerum, D. B. Rorabacher and J. F. G. Clarke Jnr., *Inorg. Chem*, 1963, **2**, 667.
29 N. F. Hall and M. R. Spinkle, *J. Am. Chem. Soc.*, 1932, **54**, 3469.
30 F. Rived, M. Roses and E. Bosch, *Anal. Chim. Acta*, 1998, **374**, 309.
31 Ref. 21, p. 152.
32 Ref. 23, p. 265.
33 B. G. Cox, *Acids and Bases Solvent Effects on Acid-Base Strength*, OUP, Oxford, 2013, p. 131.

